Rotating vectorial vortices produced by space-variant subwavelength gratings

Avi Niv, Gabriel Biener, Vladimir Kleiner, and Erez Hasman

Optical Engineering Laboratory, Faculty of Mechanical Engineering, Technion—Israel Institute of Technology, Haifa 32000, Israel

Received May 5, 2005; revised manuscript received June 26, 2005; accepted July 13, 2005

A new class of vectorial vortex based on coherent addition of two orthogonal circularly polarized Bessel beams of identical order but with different propagation constants is presented. The transversely space-variant axially symmetric polarization distributions of these vectorial fields rotate as they propagate, while they maintain a propagation-invariant Bessel intensity distribution. These properties were demonstrated by use of discrete space-variant subwavelength gratings for 10.6 μm CO_2 laser radiation. The polarization properties were verified by both full space-variant polarization analysis and measurements. Rotating intensity patterns are also demonstrated by transmitting the vectorial vortices through a linear polarizer.

OCIS codes: 260.5430, 050.2770, 230.5440.

Singularities in scalar wave fields appear at points or along lines where the phase or the amplitude of the wave either is undefined or abruptly changes. One class of singularities is the scalar vortex, which is a spiral phase ramp around a singularity.[1] Until now, researchers had focused mainly on scalar vortices.[2] However, if we allow the polarization to be space varying, vectorial vortices may appear.[3–6] A vectorial vortex occurs around a point where a scalar vortex is centered in at least one of the scalar components of the vectorial wave field. Vectorial vortices are found in the vectorial fields proposed by Pääkkönen *et al.*[7] and at the center of vectorial Bessel beams.[8]

In this Letter we propose and demonstrate a novel set of paraxial beams containing rotating vectorial vortices. The polarization state of these vectorial vortices rotates on propagation, while an intensity distribution is maintained that is axially symmetric and propagation invariant. The vectorial field is analyzed by use of a stationary phase approximation. Demonstration is obtained for 10.6 μm CO_2 laser radiation by fabrication of discrete (piecewise-continuous) space-variant subwavelength gratings. The vectorial vortices were investigated by measuring the polarization state at various locations along the propagation axis of the resulting beams. Finally, rotating intensity patterns were demonstrated by transmitting the vectorial vortices through a linear polarizer.

The polarization state of a monochromatic wave is characterized by two parameters, the ellipticity and the azimuthal angle of the polarization ellipse.[9] Propagation-dependent rotation of the azimuthal angle can be obtained by superimposing orthogonal circularly polarized Bessel beams of identical order but with different propagation constants. Such beams result from a field of the form

$$|E\rangle = \frac{1}{\sqrt{2}}\{\exp[im\varphi - ik(\beta-\alpha)r]|R\rangle + \exp[-im\varphi - ik(\beta+\alpha)r]|L\rangle\}. \quad (1)$$

In this case (r,φ) are polar coordinates, m is an integer, and α and β are real constants with $\alpha<\beta$ and $k=2\pi/\lambda$. Right- or left-handed circular polarization is represented by $|R\rangle$ and $|L\rangle$, respectively. Each of the beam's scalar components contains a vortex of equal charge and opposite sign. Using stationary phase approximation,[7] the Fresnel propagation integral of this complicated space-variant polarized beam yields

$$|E(r,\varphi,z)\rangle = A(r,z)\{(\beta-\alpha)J_m[k(\beta-\alpha)r] \times\exp[i(m\varphi + k\alpha\beta z)]|R\rangle + (\beta+\alpha) \times J_m[k(\beta+\alpha)r]\exp[-i(m\varphi + k\alpha\beta z)]|L\rangle\}, \quad (2)$$

where $A=\pi\sqrt{z/\lambda}\exp\{ik[z+r^2/2z-(\alpha^2+\beta^2)z/2]\}$ and J_m represents the mth-order Bessel function of the first kind. Thus we find in the paraxial regime a beam that is the coherent addition of collinear, identically ordered and orthogonally polarized Bessel beams, with different arguments and magnitudes and with spiral phases. By definition, then, the beam is a vectorial vortex. Significantly, as the scalar components have different propagation constants, they accumulate phase differences (retardation) as the vectorial vortex propagates. From Eq. (2), the retardation is given by $\Delta\phi=2(m\varphi+k\alpha\beta z)$. This equation shows that lines with constant retardation have a spiral form. As a result, the azimuthal angle of the polarization rotates as the beam propagates, thereby producing a rotating vectorial vortex. A full rotational cycle is obtained for $\Delta\phi=2\pi$, which corresponds to the propagation distance denoted by $z_T=\pi/(k\alpha\beta)$. From $A(r,z)$ we find a linear growth of the intensity as the beam propagates. However, this growth can easily be removed by appropriate apodization of the incoming beam.[10] Figure 1(a) shows the calculated intensity of a vectorial vortex with $m=1$, $\alpha=0.0053$, $\beta=0.0122$, and wavelength $\lambda=10.6$ μm at a propagation distance of $z/z_T=0.5$. An axially symmetric in-

0146-9592/05/212933-3/$15.00

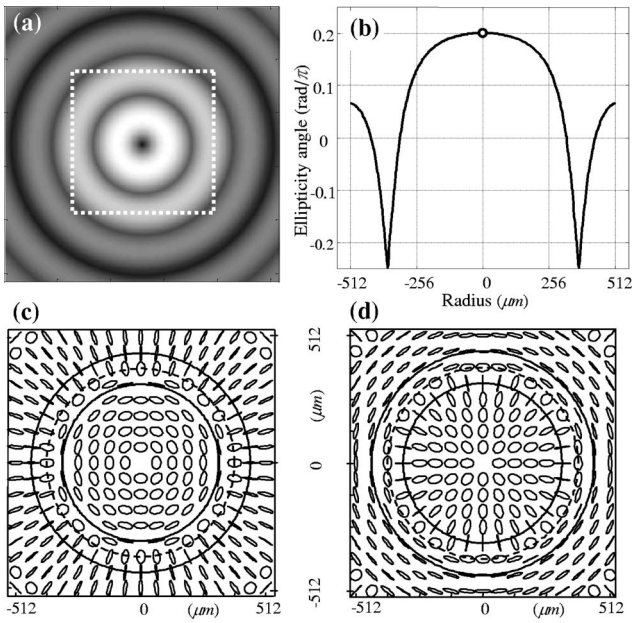

Fig. 1. Simulation results for $m=1$. (a) Normalized intensity pattern. (b) Radial dependence of the ellipticity angle; empty circle indicates singularity. (c), (d) Local polarization ellipses for propagation distances $z/z_T=0,0.5$, respectively. The domain size is shown by the dotted square in (a). The concentric solid and dashed circles indicate the locations of linear and circular polarization, respectively.

tensity distribution is clearly observed. From Ref. 9, ellipticity angle χ and orientation angle ψ of the field in Eq. (2) are given by

$$\sin(2\chi) = \frac{(\beta-\alpha)^2 J_m{}^2[k(\beta-\alpha)r] - (\beta+\alpha)^2 J_m{}^2[k(\beta+\alpha)r]}{(\beta-\alpha)^2 J_m{}^2[k(\beta-\alpha)r] + (\beta+\alpha)^2 J_m{}^2[k(\beta+\alpha)r]}, \tag{3a}$$

$$\psi_{\mathrm{mod}\,\pi} = k\alpha\beta z + m\varphi + \frac{\pi}{2}\vartheta\{J_m[k(\beta-\alpha)r] \times J_m[k(\beta+\alpha)r]\}, \tag{3b}$$

where $\vartheta\{\,\}$ denotes the Heaviside step function. From Eq. (3a) we find the ellipticity to be axially symmetric, while Eq. (3b) indicates that the polarization ellipse rotates uniformly as the vectorial vortex propagates. At the core of the vectorial vortex, both the ellipticity and the orientation of the polarization ellipse are undefined, and the intensity takes on a null value (dark C point in Ref. 5). This is a typical occurrence with a vectorial vortex in which both scalar components contain a vortex. In Fig. 1(b) the radial dependence of the ellipticity is plotted for $m=1$. At 322 and 434 μm the ellipticity is zero and the polarization state is linear. At 370 μm the ellipticity is $-\pi/4$; hence the polarization is right-handed circular. Azimuthal angle ψ is undefined at locations of circular polarization; hence $\pi/2$ jumps in Eq. (3b). Figures 1(c) and 1(d) show the calculated local polarization ellipses for an $m=1$ vectorial vortex in the vicinity of the core for $z/z_T=0$ and $z/z_T=0.5$, respectively. The area of simulation is indicated by the white square in Fig. 1(a). The concentric solid and dashed circles indicate the locations of linear (L lines) and circular (C lines) polarizations, respectively.[5] Rotation of the polarization ellipses according to Eq. (3b), as well as the $\pi/2$ jumps, are clearly observed. Also, the L lines separate areas of different handedness, as is evident from Fig. 1(b).[4] We note that choosing a different set of orthogonal polarization states in Eq. (1) produces different evolution of the polarization states; e.g., superimposing orthogonal linear polarizations results in a rotation in ellipticity angle χ.

Rotating vectorial vortices are easily generated by use of space-variant subwavelength gratings. It was found previously[11] that under linearly polarized plane-wave illumination the Jones vector of a beam emerging from a π retardation space-variant subwavelength grating is given by $|E_{\mathrm{out}}\rangle=(1/\sqrt{2})\times\{\exp[i2\theta(r,\varphi)]|R\rangle+\exp[-i2\theta(r,\varphi)]|L\rangle\}$, where $\theta(r,\varphi)$ is the local groove orientation and perfect transmission has been assumed. $|E_{\mathrm{out}}\rangle$ comprises two orthogonal, circularly polarized waves; whereby the phase of each wave results from manipulation of the space-variant polarization state and therefore is geometric in nature.[11,12] By choosing $\theta=(m\varphi+k\alpha r)/2$ and transmitting $|E_{\mathrm{out}}\rangle$ through an axicon whose phase function is $\exp(-ik\beta r)$, we were able to generate the desired field of Eq. (2). According to our approach, the groove orientation is approximated by $\theta(r,\varphi)_{\mathrm{mod}\,\pi}=F_N(m\varphi+k\alpha r)/2$, where $F_N(x)$ is a piecewise continuous function of N discrete steps.[12] We fabricated elements with $m=1,2,3,4$ upon GaAs wafers for 10.6 μm CO_2 laser radiation. The elements were 10 mm in diameter, with a 2 μm local subwavelength period and $N=16$. The parameter $\alpha=0.0053$ was chosen to obtain $z_T=82$ mm, using $\beta=0.0122$ as the refractive axicon. The elements were etched to a nominal depth of 5 μm to achieve the desired π retardation. For these elements more than 98% diffraction efficiency is expected.[12] For a more detailed description of the fabrication process, we recommend that the reader consult Ref. 11.

Figure 2(a) shows a scanning electron microscope

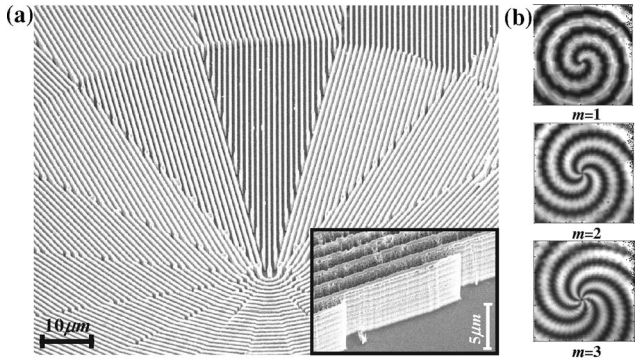

Fig. 2. (a) Scanning electron microscope image of the element for $m=1$; inset, grooves of the subwavelength grating. (b) Measured intensity distributions of linearly polarized illumination imaged through a linear polarizer immediately behind the elements for $m=1,2,3$.

image of the $m=3$ subwavelength grating. The discrete changes in the groove orientation along the radial and azimuthal directions are clearly observed. Note the high aspect ratio ($\sim 1:5$) and the rectangular shape of the grooves (shown in the inset). In Ref. 11 the birefringent parameters of this type of subwavelength grating were found to be 0.74 and 0.86 for the amplitude transmissions in the directions parallel and perpendicular, respectively, to the subwavelength grooves, with a retardation phase of 0.97π. Figure 2(b) shows the intensity immediately behind the elements for linearly polarized illumination, as imaged through a linear polarizer. The fringes indicate the space-variant polarization state. Subsequently, the axicon was inserted behind the subwavelength grating and the full polarization state of the vectorial vortex was measured at various locations behind the axicon by the four-measurement technique.[9] Figure 3 shows the measured intensity and azimuthal angle in the vicinity of the inner L line (Fig. 1) at various distances behind the axicon. The standard deviation of the azimuthal angle with respect to its desired value was found to be 3% at 72 mm behind the axicon for $m=1$, thus confirming our predictions. Note that full rotation of the polarization state was obtained at the predicted propagation distance of 82 mm. The distortion in the round shape of the vectorial vortex (including the small amount of intensity in the center) shown in Figs. 3(a) and 3(c) results from linearly polarized wave perturbation caused by deviations of the birefrigent parameters with respect to their desired values.

Finally, the rotating vectorial vortices were transmitted through a linear polarizer, producing a scalar rotating beam whose intensity is given by

$$I = \frac{z}{8\lambda}\{(\beta+\alpha)^2 J_m{}^2[k(\beta+\alpha)r] + (\beta-\alpha)^2 J_m{}^2[k(\beta-\alpha)r] + 2(\beta^2-\alpha^2) J_m[k(\beta+\alpha)r] J_m[k(\beta-\alpha)r] \times \cos(2m\varphi + 2k\alpha\beta z)\}. \quad (4)$$

Figure 4 shows the calculated braided intensity structure for $m=1,3$ along with some experimental intensity images captured along the propagation axis

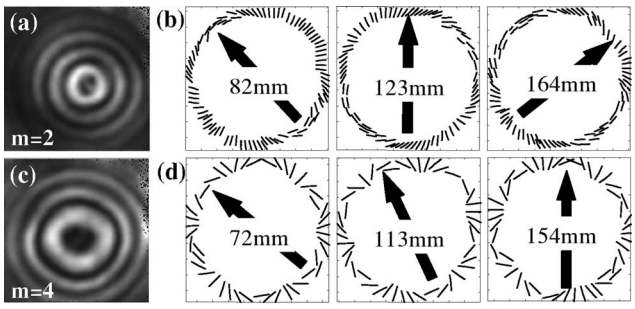

Fig. 3. (a), (c) Measured intensity distributions for $m=2,4$, respectively. (b) Measured azimuthal angle in the vicinity of the linear polarization circle at various distances behind the axicon for $m=2$. (d) Same as (b) but for $m=4$.

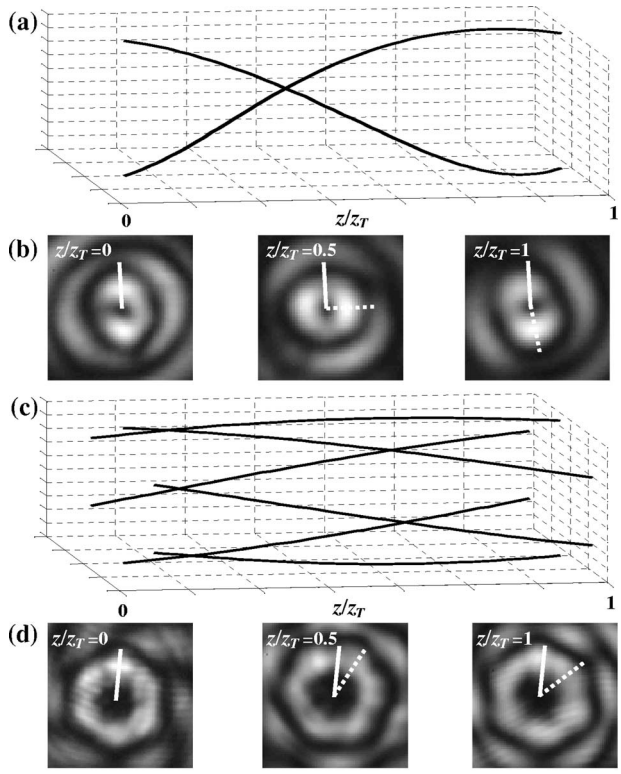

Fig. 4. (a), (c) Calculated braided intensity for $m=1,3$, respectively. (b), (d) Corresponding measured intensity distributions at different location along the braid. Solid and dashed lines introduce the rotation of the patterns.

of the beams. Rotation of the intensity pattern is clearly observed. Also note that full rotation of the intensity pattern is obtained exactly at the same distance, z_T.

E. Hasman's e-mail address is mehasman@tx.technion.ac.il.

References

1. M. S. Soskin and M. V. Vanetsov, in *Progress in Optics*, E. Wolf, ed. (North-Holland, 2001), Vol. 42, pp. 219–276.
2. D. Palacios, D. Rozas, and G. A. Swartzlander Jr., Phys. Rev. Lett. **88**, 103902 (2002).
3. J. F. Nye, Proc. R. Soc. London Ser. A **387**, 105 (1983).
4. J. F. Nye, Proc. R. Soc. London Ser. A **389**, 279 (1983).
5. I. Freund, M. Soskin, and A. I. Mokhun, Opt. Commun. **208**, 223 (2002).
6. O. Angelsky, A. Mokhun, I. Mokhun, and M. Soskin, Opt. Commun. **207**, 57 (2002).
7. P. Pääkkönen, J. Tervo, P. Vahimaa, J. Turunen, and F. Gori, Opt. Express **10**, 949 (2002).
8. A. Niv, G. Biener, V. Kleiner, and E. Hasman, Opt. Lett. **29**, 238 (2004).
9. E. Collett, *Polarized Light* (Marcel Dekker, 1993).
10. N. Davidson, A. A. Friesem, and E. Hasman, Opt. Commun. **88**, 326 (1992).
11. A. Niv, G. Biener, V. Kleiner, and E. Hasman, Opt. Commun. **251**, 306 (2005).
12. E. Hasman, G. Biener, A. Niv, and V. Kleiner, in *Progress in Optics*, E. Wolf, ed. (North-Holland, 2005), Vol. 47, pp. 215–289.